Influence of hydrogen on grid investments for smart microgrids

Bartels, Emiel Aurelius; Pippia, Tomas; De Schutter, Bart

DOI
10.1016/j.ijepes.2022.107968

Publication date
2022

Document Version
Final published version

Published in
International Journal of Electrical Power and Energy Systems

Electrical Power and Energy Systems 141 (2022) 107968

Contents lists available at ScienceDirect

International Journal of Electrical Power and Energy Systems

journal homepage: www.elsevier.com/locate/ijepes

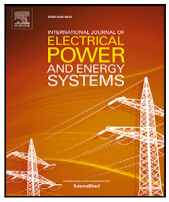

Influence of hydrogen on grid investments for smart microgrids

Emiel Aurelius Bartels *, Tomas Pippia, Bart De Schutter

Delft Center for Systems and Control, Delft University of Technology, Mekelweg 2, Delft, The Netherlands

ARTICLE INFO

Keywords:
Demand response
Electric vehicles
Hydrogen
Microgrid
Model predictive control

ABSTRACT

Electrification of the heat network in buildings together with a rise in popularity of Electric Vehicles (EVs) will result in a need to make investments in the electrical energy infrastructure in order to prevent congestion. This paper discusses the influence of hydrogen in future smart microgrids on these investments. Moreover, smart control strategies, i.e., EV management and demand response programs are used in this paper to lower the peak of electrical energy demand resulting in the reduction of these investments. Performances of microgrid with different levels of hydrogen penetration are discussed. It is shown that an increase in the level of hydrogen in the microgrid will reduce the electric grid investments costs but is not economically more beneficial than using 'green' gas due to the higher total economic costs.

1. Introduction

1.1. Literature background

In 2015, 195 governments signed an agreement for a long-term goal of keeping the increase of the global average temperature this century below two degrees and aiming for an increase of a maximum of one and a half degrees, the Paris agreement [1]. To prevent exceeding this maximum of two degrees increase of the global average temperature, scientists have determined that human society needs to reduce the amount of electricity produced by burning fossil fuels from 70% in 2010 to 20% in 2050 [2]. Therefore, more energy needs to be produced by renewable energy sources, because they have no emission of greenhouse gases. However, due to the intermittent nature of these renewable energy resources, there is a rise of complexity for the energy management [3] and a need for more flexibility in the energy grid [4].

The implementation of microgrids seems to be a possible solution to increase the integration of these renewable energy resources in the energy grid due to their ability to reduce peak demand and energy costs [5]. Microgrids consist of interconnected loads, distributed energy resources, and energy storage systems. These microgrids can be seen as a miniature version of the larger utility grid that can exchange energy with the utility grid [6]. Microgrids can provide many benefits, including improved reliability, power quality, and reduced distribution losses are realised [7,8].

Furthermore, changes are happening in the transportation sector as well to reduce the emission of greenhouse gases by replacing internal combustion engine vehicles with Electric Vehicles (EVs). The increased use of EVs has a strong effect on the demand of energy in the microgrid due to their relatively high consumption of energy [8]. This increase in energy demand in the microgrid results in the need for economic investments in the infrastructure of the microgrid since during peak consumption hours the current infrastructure will not be able to cope with the rising energy demand [9]. Therefore, in future microgrids, the focus for economic profit should be on the peak of electrical energy transfer between the microgrid and utility grid.

The impact of the increasing energy demand by the addition of EVs in the microgrid can be reduced by using smart charging strategies where the EVs can be charged when there is an abundance, or less shortage, of energy in the microgrid. Moreover, EVs can contribute to mitigate the problem of energy distribution in the microgrid by using them as a power plant or energy storage system to provide energy at times of high energy demand in the microgrid [8,10–12]. Another strategy is the use of Demand Response (DR) programs where the consumption pattern of the consumers in the microgrid is altered [13,14]. Instead of changing the energy supply one changes the demand within the microgrid to satisfy the balance of energy supply and consumption. The use of DR programs has proven to generate more flexibility in the grid and to reduce the electrical energy peak transfer [7,15].

At the same time, a new source of energy is emerging in both the energy and transportation sector, namely hydrogen [16,17]. The popularity of hydrogen is expected to increase in the next years due to its storage capabilities and cheap transport of energy. Furthermore, it can be produced without the emission of greenhouse gases [18]. Hydrogen offers a great solution to the distribution of generated renewable energy, e.g., when energy is generated on offshore wind farms and has to be transported to the consumers onshore. Fuel cell EVs are emerging

* Corresponding author.
E-mail address: emiel.bartels@gmail.com (E.A. Bartels).

https://doi.org/10.1016/j.ijepes.2022.107968
Received 11 June 2021; Received in revised form 30 November 2021; Accepted 10 January 2022
Available online 15 March 2022

due to some beneficial specifications compared to the nowadays more used battery EVs, e.g., larger range and faster refuelling [16,19,20]. The introduction of hydrogen in the microgrid can alter the behaviour of the microgrid, altering the peak of electrical energy transfer between the microgrid and utility grid. In this paper, future microgrids are considered based on the year 2050 in the Netherlands where it is assumed that hydrogen has widely emerged in the energy infrastructure. Different levels of penetration of hydrogen in the microgrid are compared to investigate the effect on required electrical grid investments.

The microgrids considered in this paper will be controlled with the Model Predictive Control (MPC) framework, which has proven to provide good performance for the energy management of a microgrid [10,21–26]. Furthermore, a Mixed Logical Dynamical (MLD) framework [27] is used to describe the dynamics of the model of the microgrid, resulting in a mixed-integer linear programming problem.

1.2. Contributions

The contribution of this paper is twofold. First, a realistic future residential hydrogen-based energy infrastructure and advanced forecasting models for the stochastic processes are constructed. It is showed how different components of the microgrid can cooperate with each other to manage the energy flow and supply different sources of energy within a future microgrid. Secondly, this paper aims to provide a primary indication of the difference in the economic costs and reduction of the peak of electrical energy transfer of the microgrid when hydrogen is introduced. The influence of hydrogen in a microgrid is simulated and discussed. In this paper, new research topics are included, such as:

- Including and evaluating different levels of hydrogen penetration in a microgrid.
- Making a comparison between performance in the microgrid including both battery and fuel cell EVs.
- Modelling energy flow in a future-based fully renewable microgrid.

To the best of the authors' knowledge this paper is the first to indicate the performance difference while injecting hydrogen in a microgrid containing both battery and fuel cell EVs. With this paper, the foundation is set to build upon to investigate what the differences are when injecting hydrogen to a microgrid and how we can use this to mitigate energy management problems in an urban microgrid.

1.3. Outline

The remainder of this paper is organised as follows. In Section 2 the key features of the microgrid and its model are presented. In Section 3, the different forecasting models that are used to forecast the stochastic processes in the microgrid are discussed. In Section 4, the control objective and the MPC framework are presented. Scenarios with different levels of hydrogen penetration are compared and discussed. Some final conclusions and suggestions for future work are given in Section 6.

2. Microgrid modelling

In this section, we describe the key features of the microgrid, which comprises discrete-time dynamics of the distributed energy resources and energy flows. We remark that a constant ratio between energy and power per time step is assumed due to the constant sampling time $\Delta T = T(k+1) - T(k)$. A future microgrid is constructed based on predictions in the Dutch energy infrastructure in 2050 [28]. In this future microgrid, a level of penetration of hydrogen can be considered, resulting in a relatively vast share of hydrogen-based components in the microgrid. Therefore, an electrolyser with hydrogen storage tank and fuel cell EVs are assumed to be present as seen in Fig. 1. Since there will be a scenario considered without hydrogen in the microgrid, as will be explained in Section 5, 'green' gas can flow through the gas infrastructure instead of hydrogen as well. Furthermore, a microgrid with residential and small commercial consumers is considered with a high usage of Photovoltaic (PV) panels. The remainder of this section will elaborate on the working principle, models, and energy balances in this microgrid.

2.1. Components in the microgrid

For the different components in the microgrid, the working principle and the models of the different components in the microgrid are described.

2.1.1. Battery

The battery serves as energy storage system where energy can be temporarily stored or consumed from to compensate for the discrepancies in the supply and demand of energy in the microgrid. The dynamics that describe the stored energy in a battery x_{bat} at the next time step $k+1$ depend on the mode the battery is in, i.e., charging or discharging mode. A binary variable is introduced such that $\delta_{\text{bat}}(k) = 1$ if the battery is charging and $\delta_{\text{bat}}(k) = 0$ if the battery is discharging at time step k. It is necessary to model the battery using this binary variable due to the difference in charging and discharging efficiency. Therefore, the dynamics of the battery are being described as:

$$x_{\text{bat}}(k+1) = \begin{cases} x_{\text{bat}}(k) + \eta_{\text{c}} u_{\text{bat}}(k), & \text{if } \delta_{\text{bat}}(k) = 1 \\ x_{\text{bat}}(k) + \frac{1}{\eta_{\text{d}}} u_{\text{bat}}(k), & \text{if } \delta_{\text{bat}}(k) = 0 \end{cases},$$

where u_{bat} is the exchanged electrical energy, η_{c} the charging efficiency, and η_{d} the discharging efficiency. The state of the battery and the electrical energy exchanged to or from the battery cannot exceed their minimal and maximal bounds. Therefore, the constraints $\underline{x}_{\text{bat}} \leq x_{\text{bat}}(k) \leq \overline{x}_{\text{bat}}$ and $\underline{u}_{\text{bat}} \leq u_{\text{bat}}(k) \leq \overline{u}_{\text{bat}}$ apply. Moreover, an extra constraint on the energy transfer is set to distinguish whether energy is coming in or leaving the battery, i.e., whether the battery is in charging or discharging mode. Therefore, $\delta_{\text{bat}}(k) = 1 \iff u_{\text{bat}}(k) \geq 0$.

2.1.2. Hydrogen storage tank

Remaining hydrogen in the microgrid can be temporarily stored in the hydrogen storage tank to be used at a later time. The amount of hydrogen stored in the tank x_{hst} at time step $k+1$ is proposed to be modelled as

$$x_{\text{hst}}(k+1) = x_{\text{hst}}(k) + u_{\text{hst}}(k),$$

where $u_{\text{hst}}(k)$ is the hydrogen exchanged at time step k. Similarly to the battery case, bounds are set on the amount of stored and exchanged hydrogen, i.e., $\underline{x}_{\text{hst}} \leq x_{\text{hst}}(k) \leq \overline{x}_{\text{hst}}$ and $\underline{u}_{\text{hst}} \leq u_{\text{hst}}(k) \leq \overline{u}_{\text{hst}}$.

2.1.3. Electrolyser

The electrolyser converts the consumed electrical energy u_{elc} into hydrogen H_{elc} when the system is on $\left(u_{\text{elc}}(k) = 1\right)$. When the system is off $\left(u_{\text{elc}}(k) = 0\right)$, the electrolyser will not produce any hydrogen. Therefore, the microgrid can generate its own hydrogen when needed when there is a redundancy of electrical energy instead of importing hydrogen from the utility grid. The electrolyser can be written as

$$H_{\text{elc}}(k) = \alpha_{\text{elc}} u_{\text{elc}}(k),$$

where α_{elc} is a model parameter related to the specifications of the system as proposed in [10]. The amount of electrical energy that is consumed is constrained by $0 \leq u_{\text{elc}}(k) \leq \overline{u}_{\text{elc}}$.

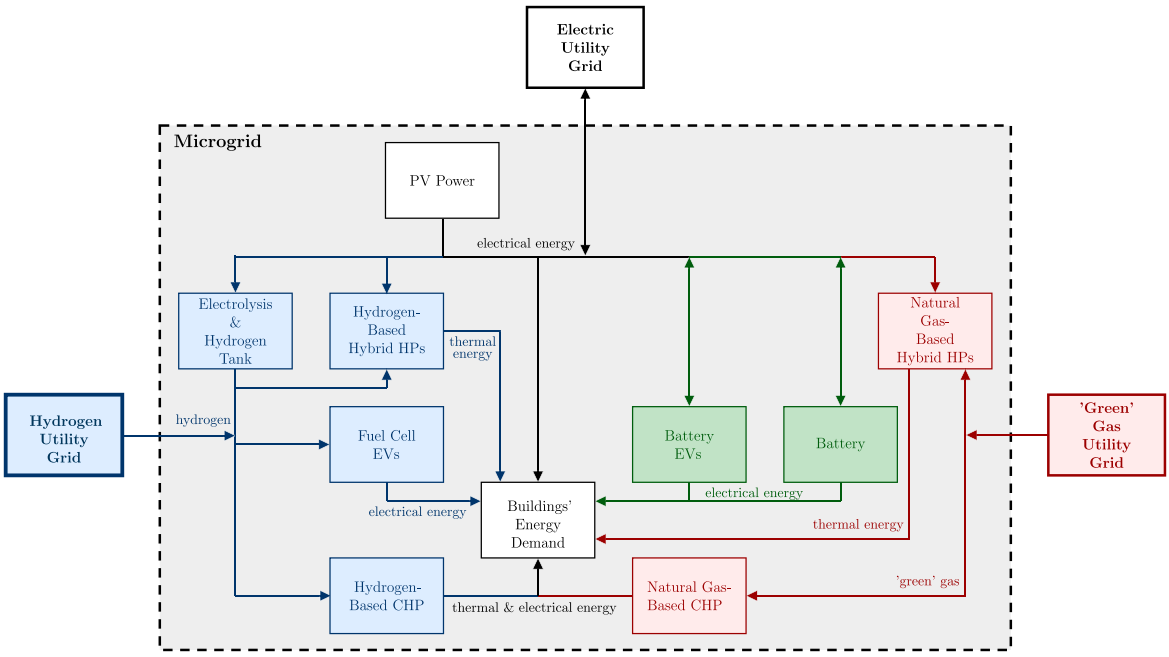

Fig. 1. Visualisation of the scenarios considered in the case studies, with Electric Vehicles (EVs), Photovoltaic (PV) power, Heat Pumps (HP), and micro-Combined Heat and Power (μ-CHPs) plants. The white boxes are included in each scenario. The electric scenario is constructed by adding the red and green parts, the mixed scenario by adding the blue part and green parts, and the hydrogen scenario by only including the blue part.

2.1.4. PV power

The power coming from the PV panels is calculated as a function of the solar irradiance and ambient temperature following [29] as

$$P_{\mathrm{PV}}(k) = P_{\mathrm{STC}} \frac{G_{\mathrm{c}}(k)}{G_{\mathrm{STC}}} \left[1 + \alpha \left(T_{\mathrm{c}}(k) - T_{\mathrm{STC}}\right)\right], \quad \text{with}$$
$$T_{\mathrm{c}}(k) = T_{\mathrm{amb}}(k) + (T_{\mathrm{NOCT}} - 20)\frac{G_{\mathrm{c}}(k)}{800}. \tag{1}$$

The nominal power P_{STC}, the global irradiance G_{STC}, and the cell temperature T_{STC} are determined under standard test conditions of (1000 W/m^2, 25 °C). The air mass coefficient that is commonly used to characterise the performance of solar cells under the standardised conditions (P_{STC}) is assumed to be AM1.5. This is almost universal when characterising terrestrial PV panels [30]. Furthermore, α is the negative power temperature coefficient, and T_{NOCT} the nominal operating cell temperature. These values are commonly given by the manufacturers of the PV panels. The global irradiance $G_{\mathrm{c}}(k)$ and ambient temperature $T_{\mathrm{amb}}(k)$ at time step k are estimated to calculate the cell temperature $T_{\mathrm{c}}(k)$ and generated PV power $P_{\mathrm{PV}}(k)$.

2.1.5. Hybrid heat pump

The hybrid heat pump can produce thermal energy Q_{HP} by consuming electrical energy $u^{\mathrm{el}}_{\mathrm{HP}}$ or gas $u^{\mathrm{th}}_{\mathrm{HP}}$. When the outside temperature is high enough, the built-in heat pump will retrieve the outside air to warm up the house. Otherwise, gas is burned to heating the house, which is less energy efficient. Therefore, two logic binary variables are introduced to represent whether at time step k the hybrid heat pump is running on electrical energy $\left(\delta^{\mathrm{el}}_{\mathrm{HP}}(k) = 1\right)$, on thermal energy $\left(\delta^{\mathrm{th}}_{\mathrm{HP}}(k) = 1\right)$, or if the system is off $\left(\delta^{\mathrm{el}}_{\mathrm{HP}}(k) = \delta^{\mathrm{th}}_{\mathrm{HP}}(k) = 0\right)$. Therefore, the hybrid heat pump is being modelled in this paper as

$$Q_{\mathrm{HP}}(k) = \begin{cases} \eta^{\mathrm{el}}_{\mathrm{HP}} u^{\mathrm{el}}_{\mathrm{HP}}(k), & \text{if } \delta^{\mathrm{el}}_{\mathrm{HP}}(k) = 1 \text{ and } \delta^{\mathrm{th}}_{\mathrm{HP}}(k) = 0 \\ \eta^{\mathrm{th}}_{\mathrm{HP}} u^{\mathrm{th}}_{\mathrm{HP}}(k), & \text{if } \delta^{\mathrm{el}}_{\mathrm{HP}}(k) = 0 \text{ and } \delta^{\mathrm{th}}_{\mathrm{HP}}(k) = 1 \\ 0, & \text{if } \delta^{\mathrm{el}}_{\mathrm{HP}}(k) = \delta^{\mathrm{th}}_{\mathrm{HP}}(k) = 0 \end{cases}$$

where $\eta^{\mathrm{el}}_{\mathrm{HP}}$ is the electrical efficiency and $\eta^{\mathrm{th}}_{\mathrm{HP}}$ the efficiency of burning hydrogen. The maximal consumed energy is constrained by the equations $0 \leq u^{\mathrm{el}}_{\mathrm{HP}}(k) \leq \overline{u}^{\mathrm{el}}_{\mathrm{HP}}$ and $0 \leq u^{\mathrm{th}}_{\mathrm{HP}}(k) \leq \overline{u}^{\mathrm{th}}_{\mathrm{HP}}$. The consumption of energy, either electrical or gas, will be zero if that mode is off, i.e., $\delta^{\mathrm{el}}_{\mathrm{HP}}(k) = 0 \iff u^{\mathrm{el}}_{\mathrm{HP}}(k) = 0$ and $\delta^{\mathrm{th}}_{\mathrm{HP}}(k) = 0 \iff u^{\mathrm{th}}_{\mathrm{HP}}(k) = 0$. Since the hybrid heat pump will not consume electrical energy and use the boiler at the same time, a constraint is added such that the logical binary variables cannot both be equal to one at time step k, i.e., $\delta^{\mathrm{el}}_{\mathrm{HP}}(k) + \delta^{\mathrm{th}}_{\mathrm{HP}}(k) \leq 1$.

2.1.6. Micro-combined heat and power plant

The micro-Combined Heat and Power (μ-CHP) plant generates electrical P_{CHP} energy and also saves the otherwise wasted thermal energy Q_{CHP} during the generation by water or air heating simultaneously. Moreover, a thermal storage unit is included where energy can be stored x_{CHP}. The production of energy depends on the amount of consumed gas u_{CHP}. This concludes to the dynamics of a μ-CHP plant being described as

$$P_{\mathrm{CHP}}(k) = \eta^{\mathrm{el}}_{\mathrm{CHP}} u_{\mathrm{CHP}}(k)$$
$$x_{\mathrm{CHP}}(k+1) = x_{\mathrm{CHP}}(k) + \eta^{\mathrm{th}}_{\mathrm{CHP}} u_{\mathrm{CHP}}(k) - Q_{\mathrm{CHP}}(k),$$

where $\eta^{\mathrm{el}}_{\mathrm{CHP}}$ and $\eta^{\mathrm{th}}_{\mathrm{CHP}}$ are the electrical and thermal efficiency of the plant. The consumed energy and stored energy are bounded by $0 \leq u_{\mathrm{CHP}}(k) \leq \overline{u}_{\mathrm{CHP}}$ and $\underline{x}_{\mathrm{CHP}} \leq x_{\mathrm{CHP}}(k) \leq \overline{x}_{\mathrm{CHP}}$. The minimum stored thermal energy needs to be higher than a determined threshold $\underline{x}_{\mathrm{CHP}} > 0$.

2.2. Electric vehicles

Smart EV management can be implemented in a microgrid where smart charging or refuelling of the EV is done and the EV can be used as an energy storage system or power plant when parked. Due to these strategies, a microgrid can be more flexible and self-sustainable, i.e., less power exchange with the utility grid will be needed [10,31–33]. Moreover, the EV can provide energy in times of large demand for energy, reducing the peak of electrical energy demand [31]. In this study, vehicle-to-grid is chosen since a microgrid with a large number of EVs is considered and it is assumed that in a future scenario, such an implementation will be possible. Moreover, this strategy can provide the most reduction in the peak of electrical energy demand [32,33].

2.2.1. Battery EV

The battery EV dynamics are based on the dynamics of the battery but they include more modes since the EV can be in transportation. The EV can be refilled with electrical energy, provide electrical energy to the microgrid, be in transportation, or arrive after its trip. The amount of electrical energy stored in the battery EV x_{BEV} is based on the electrical energy u_{BEV} transferred and the energy costs of a trip h_{BEV}. The model of the battery EV, derived from [10], can be written down as

$$x_{\mathrm{bev}}(k+1) = \begin{cases} x_{\mathrm{bev}}(k) + \eta^{\mathrm{c}}_{\mathrm{bev}} u_{\mathrm{bev}}(k), & \text{if refilling} \\ x_{\mathrm{bev}}(k), & \text{if no generation} \\ x_{\mathrm{bev}}(k) + \frac{1}{\eta^{\mathrm{d}}_{\mathrm{bev}}} u_{\mathrm{bev}}(k), & \text{if generation} \\ x_{\mathrm{bev}}(k), & \text{if transportation} \\ x_{\mathrm{bev}}(k) - h_{\mathrm{bev}}(k), & \text{if arrival} \end{cases}$$

where $\eta^{\mathrm{c}}_{\mathrm{bev}}$ and $\eta^{\mathrm{d}}_{\mathrm{bev}}$ are the charging and discharging efficiencies, respectively. Constraints are set on the total energy storage of the battery $\underline{x}_{\mathrm{bev}} \leq x_{\mathrm{bev}}(k) \leq \overline{x}_{\mathrm{bev}}$ as well as on the transferred energy $\underline{u}_{\mathrm{bev}} \leq u_{\mathrm{bev}}(k) \leq \overline{u}_{\mathrm{bev}}$. The value of the transferred energy is managed in a similar way as in the battery: $u_{\mathrm{bev}}(k) \geq 0 \iff$ refilling mode, and $u_{\mathrm{bev}}(k) < 0 \iff$ generation mode.

2.2.2. Fuel cell EV

The fuel cell EV is modelled in a similar way as the battery EV to estimate the amount of hydrogen x_{fev} in the tank. However, a difference is that the refilled energy $u^{\mathrm{hyd}}_{\mathrm{fev}}$ and trip cost h_{fev} are expressed in amounts of hydrogen, while in generation mode electrical energy $u^{\mathrm{el}}_{\mathrm{fev}}$ is produced. Furthermore, the dynamics of the battery in the battery EV are replaced by the dynamics of a fuel cell to get the model for a fuel cell EV [10]:

$$x_{\mathrm{fev}}(k+1) = \begin{cases} x_{\mathrm{fev}}(k) + u^{\mathrm{hyd}}_{\mathrm{fev}}(k), & \text{if refilling} \\ x_{\mathrm{fev}}(k), & \text{if no generation} \\ x_{\mathrm{fev}}(k) - \left(\alpha_{\mathrm{fev}} u^{\mathrm{el}}_{\mathrm{fev}}(k) + \beta_{\mathrm{fev}}\right), & \text{if generation} \\ x_{\mathrm{fev}}(k), & \text{if transportation} \\ x_{\mathrm{fev}}(k) - h_{\mathrm{fev}}(k), & \text{if arrival} \end{cases}$$

where α_{fev} and β_{fev} are the model parameters of the fuel cell in the EV. These model parameters are based on the specifications of the fuel stack in the EV as described in [10,34]. Constraints are set on the hydrogen storage, transferred hydrogen, and the electrical energy transferred, i.e., $\underline{x}_{\mathrm{fev}} \leq x_{\mathrm{fev}}(k) \leq \overline{x}_{\mathrm{fev}}$, $0 \leq u^{\mathrm{hyd}}_{\mathrm{fev}}(k) \leq \overline{u}^{\mathrm{hyd}}_{\mathrm{fev}}$, and $0 \leq u^{\mathrm{el}}_{\mathrm{fev}}(k) \leq \overline{u}^{\mathrm{el}}_{\mathrm{fev}}$, respectively. The maximum generated electrical energy is based on the fact the fuel cell will operate at partial load when in generation mode.

2.2.3. Trip characteristics

A stochastic part for the EV modelling is the trip pattern as well as the fuel costs of these trips. Assumptions need to be made to model these stochastic processes. A data set with real data on the arrival and departure times of EVs and on charging patterns of EVs in the Netherlands from ElaadNL [35] has been obtained. These charging sessions can be clustered into three groups by the method described in [36]: charge-near-home, park-to-charge, and charge-near work. In this method, the charging sessions are clustered based on the duration of charging and the time of the day. Furthermore, it is shown in [36] that the arrivals are earlier in summer and spring than in autumn and winter. Moreover, people stay out of home longer during weekends resulting in later arrival times compared to the weekdays. The obtained data set is clustered and only the charge-near-home data are used to describe different arrival and departure time patterns for the EVs in the microgrid.

The energy cost per trip is calculated based on the average number of kilometres driven per year. It is assumed that the driving behaviour will not change when switching from internal combustion engine vehicles to EVs, and that the average number of kilometres driven per trip is 35.57 in the Netherlands. From [36], it is estimated that 54.4% of the charging sessions are charge-near-home sessions. Therefore, not all the energy for the EV will be refilled in the microgrid, but also at work or in public charging poles elsewhere. It is assumed that 19.35 kilometres worth of fuel is the average energy cost per trip for the EVs in the microgrid. Since different vehicles will have different driving patterns, a multivariate random Gaussian sampling with a mean of 1 and standard deviation of 0.5 is used to obtain different trip costs for different EVs.

2.3. Demand response

Direct load control is implemented in the microgrid as a DR program since it can provide good performance in lowering the peak of electrical energy transfer and is suitable for the low-consumption consumers considered in the microgrid. It is assumed that only residential consumers are willing to participate in the DR program.

2.3.1. Curtailable load

Curtailable load D_{c} can temporarily be lowered or switched off. The decision variable $\beta_{\mathrm{c}}(k)$ with $0 \leq \beta_{\mathrm{c}}(k) \leq 1$ expresses the percentage of preferred power level to be curtailed at time step k. Thus, if no curtailment is allowed, $\beta_{\mathrm{c}}(k) = 0$ at time step k [22]. Only the thermal energy is considered to be applicable for curtailment against some discomfort costs, i.e., the temperature in the building becomes lower than preferred (or higher in hot climates). Note that only a fraction of the thermal energy demand will be considered to be available for curtailment. The curtailed load Q_{c} is expressed by

$$Q_{\mathrm{c}}(k) = \beta_{\mathrm{c}}(k) D_{\mathrm{c}}(k).$$

2.3.2. Reschedulable load

Reschedulable loads D_{r} can be shifted in time, but in contrast to the curtailable loads, there corresponding energy demand has to be consumed before a certain time. These loads are divided into two different subcategories: uninterruptible and interruptible loads. In this paper, only uninterruptible loads are considered since no data of large consumption interruptible household devices were available. However, the smart charging of EVs due to the implementation of the EV management strategies can be considered as an interruptible load in the microgrid. The approach for interruptible load is similar to that of uninterruptible load despite from the fact that no constraint needs to be added to ensure the corresponding energy demand is consumed in one go.

Both fractions of the electrical and thermal energy are considered to be reschedulable. The only electric devices that are considered to be reschedulable are dishwashers. These devices are chosen due to their regular consumption pattern and their time of use. Dishwashers are used in the evening where, in general, large peaks of electrical energy demand are visible. Similar to the curtailable load, a variable $\beta_{\mathrm{r}}(k)$ with $0 \leq \beta_{\mathrm{r}}(k) \leq 1$ is introduced to indicate the percentage of preferred level to be rescheduled at time step k. This results in the following equation of rescheduled load for electrical and thermal demand:

$$\begin{aligned} P_{\mathrm{r}}(k) &= \beta^{\mathrm{el}}_{\mathrm{r}}(k) D^{\mathrm{el}}_{\mathrm{r}}(k) \\ Q_{\mathrm{r}}(k) &= \beta^{\mathrm{th}}_{\mathrm{r}}(k) D^{\mathrm{th}}_{\mathrm{r}}(k) \end{aligned},$$

where P_{r} and Q_{r} are the rescheduled electrical and thermal load, respectively. The energy demands of the rescheduled loads have to be consumed at other time steps. Since these loads are uninterruptible ones, they have to be satisfied in consecutive time steps. The amount of energy that is consumed at each time step is a constant denoted as $D^{\mathrm{el}}_{\mathrm{rc}}$ or $D^{\mathrm{th}}_{\mathrm{rc}}$ for the electrical and thermal energy, respectively. A binary variable δ_{rc} is introduced to determine whether the rescheduled energy demand is consumed ($\delta_{\mathrm{rc}}(k) = 1$) or not ($\delta_{\mathrm{rc}}(k) = 0$) at time step k. This leads to the following constraint on the consumed rescheduled energy per time step:

$$\begin{aligned} P_{\mathrm{rc}}(k) &= D^{\mathrm{el}}_{\mathrm{rc}} \delta^{\mathrm{el}}_{\mathrm{rc}}(k) \\ Q_{\mathrm{rc}}(k) &= D^{\mathrm{th}}_{\mathrm{rc}} \delta^{\mathrm{th}}_{\mathrm{rc}}(k) \end{aligned},$$

where $P_{\mathrm{rc}}(k)$ and $Q_{\mathrm{rc}}(k)$ are the consumed electrical and thermal energy at time step k. The following constraints assure that the energy is consumed without interruption:

$$\delta^{\mathrm{el}}_{\mathrm{rc}}(k) - \delta^{\mathrm{el}}_{\mathrm{rc}}(k-1) \leq \delta^{\mathrm{el}}_{\mathrm{rc}}(\tau), \text{ for } \tau = k+1, \dots, k + T^{\mathrm{el}}_{\mathrm{cr}} - 1$$
$$\delta^{\mathrm{th}}_{\mathrm{rc}}(k) - \delta^{\mathrm{th}}_{\mathrm{rc}}(k-1) \leq \delta^{\mathrm{th}}_{\mathrm{rc}}(\tau), \text{ for } \tau = k+1, \dots, k + T^{\mathrm{th}}_{\mathrm{cr}} - 1$$

where $T^{\mathrm{el}}_{\mathrm{cr}}$ and $T^{\mathrm{th}}_{\mathrm{cr}}$ are the time needed for the unsatisfied rescheduled electrical $l^{\mathrm{el}}_{\mathrm{r}}$ and thermal energy demand $l^{\mathrm{th}}_{\mathrm{r}}$ to be fully consumed, respectively. To estimate how much electrical and thermal energy still needs to be consumed at time step k, the values are updated as follows:

$$l^{\mathrm{el}}_{\mathrm{r}}(k) = l^{\mathrm{el}}_{\mathrm{r}}(k-1) + P_{\mathrm{r}}(k-1) - P_{\mathrm{rc}}(k)$$
$$l^{\mathrm{th}}_{\mathrm{r}}(k) = l^{\mathrm{th}}_{\mathrm{r}}(k) + Q_{\mathrm{r}}(k-1) - Q_{\mathrm{rc}}(k)$$

The rescheduled energy demand has to be consumed before reaching a predefined time step F. For example, a dishwasher can be rescheduled in the evening to a later time step, but one wants that the program is done by the coming morning. Therefore, no unsatisfied load should be present at that time step, i.e., $l^{\mathrm{el}}_{\mathrm{r}}(F_{\mathrm{el}}) = 0$ and $l^{\mathrm{th}}_{\mathrm{r}}(F_{\mathrm{th}}) = 0$.

2.4. Connection to utility grid

The microgrid remains connected to the utility grid at all times. Therefore, it is able to import or export electrical energy, hydrogen, or 'green' gas at a certain price. To model the utility grid, a binary logic variable δ_{UG} is introduced to determine whether energy u_{UG} is bought $\left(\delta_{\mathrm{UG}}(k) = 1\right)$ or sold $\left(\delta_{\mathrm{UG}}(k) = 0\right)$ to the utility grid at time step k with $u_{\mathrm{UG}}(k) \geq 0 \iff \delta_{\mathrm{UG}}(k) = 1$. The economic cost C_{UG} for the microgrid, due the import and export of energy with the utility grid, is modelled as

$$C_{\mathrm{UG}}(k) = \begin{cases} c^{\mathrm{P}}(k) u_{\mathrm{UG}}(k), & \text{if } \delta_{\mathrm{UG}}(k) = 1 \\ c^{\mathrm{S}}(k) u_{\mathrm{UG}}(k), & \text{if } \delta_{\mathrm{UG}}(k) = 0 \end{cases},$$

where $c^{\mathrm{P}}(k)$ and $c^{\mathrm{S}}(k)$ are the purchase and sale price of energy at time step k, respectively. The transferred energy is constrained by the maximum allowed energy transfer between the microgrid and the utility grid, i.e., $\underline{u}_{\mathrm{UG}} \leq u_{\mathrm{UG}}(k) \leq \overline{u}_{\mathrm{UG}}$.

For the purchase and sale price of electricity, a time-of-use price is computed. The electrical energy price varies greatly throughout the day and shows strong weekly patterns. Therefore, an import price is computed for every time step during the week based on the national data of the Netherlands. A 20% increase in this price is added due to rising electrical energy price till the year 2050 [28]. The purchasing price of hydrogen and 'green' gas is fixed throughout the day based on the data of [28]. The sale price of energy is assumed to be equal to the net import price, i.e., excluding taxes and transportation costs.

2.5. Operational constraints

Multiple operational constraints are presented in this section.

2.5.1. Degradation

To tackle the problem of degradation for multiple components in the microgrid, a constraint is added as introduced in [22]. A constraint is set on the minimum time the system is turned on or off, i.e., T_{ON} and T_{OFF}, respectively. In this constraint, the introduced binary logic variables are used to define whether the system is on ($\delta(k) = 1$) or off ($\delta(k) = 0$). Note that in the previous section, these modes were respectively the charging and discharging mode of the battery and battery EV. The constraint is expressed without resorting to any additional variable as

$$\delta(k) - \delta(k-1) \leq \delta(\tau), \text{ for } \tau = k+1, \dots, k + T_{\mathrm{ON}} - 1$$
$$\delta(k-1) - \delta(k) \leq 1 - \delta(\tau), \text{ for } \tau = k+1, \dots, k + T_{\mathrm{OFF}} - 1$$

The first line in this equation ensures the system satisfies the minimal 'on time' and the second line the minimal 'off time'. This constraint is used to prevent fast switching between modes in the battery, electrolyser, μ–CHP, hybrid heat pump, and both types of EVs. For the hybrid heat pumps, both for thermal energy generated by electrical energy consumption and by gas, the constraint is added. Moreover, for the EVs, this constraint is introduced for both the modes refilling and generation.

2.5.2. Range anxiety

The use of EV management strategies may result in fear of the users that the EV will not be sufficiently charged upon departure, i.e., range anxiety [11]. In the model, it is chosen that it is not necessary that the EV should be fully charged upon departure since this will lead to conservative results and the exact departure time is generally not known in advance in real life. However, the following constraint is introduced to ensure a certain state of charge $\underline{x}^{\mathrm{t}}_{\mathrm{EV}}$ is reached when the vehicle turns into transportation mode $\delta^{\mathrm{t}}_{\mathrm{EV}}$:

$$x_{\mathrm{EV}}(k) \geq \underline{x}^{\mathrm{t}}_{\mathrm{EV}} \delta^{\mathrm{t}}_{\mathrm{EV}}(k),$$

where $x_{\mathrm{EV}}(k)$ is the fuel storage of the EV at time step k. Since not all trips are known beforehand, one wants to ensure as well that enough fuel is in the EV before the EV will be generating electricity to the microgrid. Therefore, another constraint is added that ensures a minimal state of charge $\underline{x}^{\mathrm{g}}_{\mathrm{EV}}$ in the EV is set before the EV can be in generation mode $\delta^{\mathrm{g}}_{\mathrm{EV}}$:

$$x_{\mathrm{EV}}(k) \geq \underline{x}^{\mathrm{g}}_{\mathrm{EV}} \delta^{\mathrm{g}}_{\mathrm{EV}}(k),$$

where $\underline{x}^{\mathrm{g}}_{\mathrm{EV}} < \underline{x}^{\mathrm{t}}_{\mathrm{EV}}$.

2.5.3. Power balance

The different types of energy sources in the microgrid have to be balanced at every time step. In the microgrid, different types of energy sources are considered: electrical energy, thermal energy, hydrogen, and 'green' gas. The power balances are given using the variables introduced in the previous section:

$$u^{\mathrm{el}}_{\mathrm{UG}}(k) + P_{\mathrm{PV}}(k) + P_{\mathrm{CHP}}(k) + u^{\mathrm{el}}_{\mathrm{fev}}(k) = P_{\mathrm{res}}(k) + P_{\mathrm{com}}(k) + P_{\mathrm{rc}}(k) - P_{\mathrm{r}}(k) + u_{\mathrm{bat}}(k) + u_{\mathrm{bev}}(k) + u_{\mathrm{elc}}(k) + u^{\mathrm{el}}_{\mathrm{HP}}(k)$$
$$Q_{\mathrm{CHP}}(k) + Q_{\mathrm{HP}}(k) = Q_{\mathrm{res}}(k) + Q_{\mathrm{com}}(k) + Q_{\mathrm{rc}}(k) - Q_{\mathrm{r}}(k) - Q_{\mathrm{c}}(k)$$
$$u^{\mathrm{gas}}_{\mathrm{UG}}(k) = u^{\mathrm{gas}}_{\mathrm{CHP}}(k) + u^{\mathrm{gas}}_{\mathrm{HP}}(k)$$
$$u^{\mathrm{hyd}}_{\mathrm{UG}}(k) + H_{\mathrm{elc}}(k) = u^{\mathrm{hyd}}_{\mathrm{CHP}}(k) + u^{\mathrm{hyd}}_{\mathrm{HP}}(k) + u^{\mathrm{hyd}}_{\mathrm{fev}}(k).$$

In the above equations, $(\cdot)^{\mathrm{el}}$, $(\cdot)^{\mathrm{gas}}$, and $(\cdot)^{\mathrm{hyd}}$ represent the energy that is generated or consumed as electricity, 'green' gas, and hydrogen, respectively. For almost all the power balances a connection to the utility grid that can act as an infinite buffer is present. The net imbalance of the microgrid can be compensated by importing or exporting (only for electricity) energy from the utility grid. The thermal power balance does not have this connection since no thermal infrastructure is present between the microgrid and utility grid. However, since the generation of thermal energy is more of a conversion of other types of energy to thermal energy, the connections to the utility grid in the other power balances act indirectly as an infinity buffer for the thermal power balance.

3. Stochastic processes

The different stochastic processes in the microgrid, i.e., PV power, electrical and thermal energy demand of residential buildings, and electrical and thermal energy demand of commercial buildings, need to be forecast to control the model described in the previous section. This section comprises an overview of the different point forecasting models for each stochastic process. Real data is used based on meteorological measurements and energy consumption patterns in the Netherlands.

3.1. Literature background

A brief description of the two forecasting models used in this paper is presented: autoregressive moving average and long short-term memory recurrent Artificial Neural Network (ANN). These models were chosen due to their good performance in the literature [37–39].

3.1.1. Autoregressive moving average

The first forecasting model used in this paper is the autoregressive moving average model based on the Box–Jenkins method [40]. This model shows reliable predictions when there exists an underlying linear correlation structure in the time series while considering the unobserved errors of previous time steps. Furthermore, a favourable aspect of the model is its flexibility since it can represent multiple types of time series by using different orders [41]. With the autoregressive moving average model, one assumes that the data do not show any characteristics of non-stationarity [37]. When non-stationary data are considered, a generalisation of the model can be used by creating an autoregressive integrated moving average model. Inherent seasonal effects of the data can be added to the model by adding seasonality to the model. Lastly, exogenous inputs with a high correlation to the forecasting data can be added to improve the performance of the model. A mathematical description of the difference autoregressive moving average models is shown in [41].

3.1.2. Artificial neural network

The second forecasting model used in this paper is the ANN. An ANN consists of multiple hidden layers making the connection from the input to the output. Each layer is composed of one or more neurons where an activation function in the neurons determines the nonlinear mapping characteristics across the ANN [42]. This approach is widely used since it does not require mathematical expressions, it is self-learning, easy to implement, short online computation time is needed, and it is able to detect complex nonlinear relations between the input and output [38]. However, drawbacks of the model are that it needs a significant amount of historical data to be properly trained and overfitting may occur [37].

In this paper, a long short-term memory recurrent ANN, as first introduced in [43], is used. A recurrent ANN is used since it considers the temporal correlation between previous information and current circumstances, resulting in that previous decisions influence the predictions in future time steps [44]. Due to the gradient vanishing or exploring in the training of the ANN by using the popular back-propagation algorithm, long-range dependencies are difficult to learn. This can be overcome by using long short-term recurrent ANNs that use a memory cell to capture these long-range dependencies, as mathematically shown in [43,44].

3.2. PV power

For the PV power, two stochastic processes need to be forecast as determined from (1), i.e., the solar irradiance and ambient temperature. Both stochastic processes are forecast in similar time steps as the available train data of one hour.

3.2.1. Solar irradiance

A clear-sky model is used since it has proven to deal with the stochastic influence of cloud covering well [45,46]. In the clear-sky model, the global horizontal solar irradiance is computed as if it was a clear-sky day G_c^{cs}, i.e., without any clouds. Therefore, the stochastic component is excluded and a clear-sky global horizontal solar irradiance can be obtained for every hour in the year. With these values, the clear-sky index θ can be computed as the normalisation of the measured solar irradiance $G_c(k)$:

$$\theta(k) = \frac{G_c(k)}{G_c^{cs}(k)}.$$

The clear-sky model is obtained from the available data, and missing data are computed using a statistical smoothing technique based on weighted quantile regressions as in [45]. In general, a limiting factor of developing clear-sky data is the absence or quality of the data [47], i.e., in the winter there are not many clear-sky observations to train the model and this increases the error of the quantile regression. This problem is partly solved by using data of the past 20 years.

It is decided from the autocorrelation of the clear-sky index that the prediction models will use data of one hour and 24 h before. Different exogenous inputs can be considered based on the geographical location [37,48] and from the data it is concluded the highest correlation coefficients for the solar irradiance are obtained with the temperature, presence of snow, and humidity. With these exogenous inputs, it is concluded that an ANN model provides the smallest root mean square error.

3.2.2. Ambient temperature

The autocorrelation is analysed and it is chosen to use the data from 1, 2, 3, 4, 5, and 24 h before for the forecasting. It is concluded that solar irradiance and humidity have the strongest correlation for temperature, but are still low. Using a seasonal autoregressive integrated moving average model provided the smallest root mean square error.

3.3. Residential energy demand

The energy demand of residential consumers is characterised by the distinctive pattern during the day, having a peak consumption in the early evening. This peak often determines the general peak in the microgrid where the electrical energy grid investments are based upon. In this section, both the electrical and thermal energy demand are forecast in the sampling time corresponding to the available data of 15 min and one hour, respectively. Since data of only one year is available and used, the ANN did not have enough training data to construct a proper model and autoregressive moving average models are used.

3.3.1. Electrical energy demand

From the autocorrelation, it is chosen that for the electrical energy demand, data of the previous 45 min and of 23:45, 24:00, and 24:15 h before is used. Exogenous inputs did not improve the models of the residential electrical energy demand. A seasonal autoregressive integrated moving average obtained the smallest root mean square error and is used in this study.

3.3.2. Thermal energy demand

Time series data of 1, 2, 23, 24, 25 h before is used, as concluded from the autocorrelation. A high correlation coefficient between the thermal energy demand and the ambient temperature is found, and the temperature is used as an exogenous input in the forecasting models. The smallest error is obtained using the seasonal autoregressive integrated moving average model.

3.4. Commercial energy demand

The commercial energy demand shows large differences in the consumption pattern between weekdays and the weekend. This is based on the opening hours of the small stores. In this section, both the electrical and thermal energy demand are forecast in the sampling time corresponding to the available data of 15 min and one hour, respectively.

3.4.1. Electrical energy demand

From an analysis of the autocorrelation, it is chosen that for the electrical energy demand, data of the previous 30 min and of 168 h before, i.e., one week ago, is used. Exogenous inputs did not improve the models of the commercial electrical energy demand. The ANN obtained the best performance, i.e., smallest root mean square error in the point forecasts.

3.4.2. Thermal energy demand

Time series data of 1, 23, 24, and 25 h before is used, as concluded from the autocorrelation. A high correlation coefficient between the thermal energy demand and the ambient temperature is found, and the temperature is used as an exogenous input in the forecasting models. The smallest root mean square error is obtained using the ANN model.

4. Control

This section discusses the objective function of the optimisation problem in the microgrid and the MPC strategy used.

4.1. Objective function

The objective function considers the economic profitability of lowering the peak of electrical energy demand (J_{gd}) as well as the energy import costs (J_{eco}). Discomfort penalties (J_{dis}) and the durability of the EVs (J_{dur}) are included as well, resulting in a multi-objective function as

$$J = \alpha J_{\text{eco}} + \beta J_{\text{dis}} + \gamma J_{\text{dur}} + \lambda J_{\text{gd}},$$

with α, β, γ, and λ being predefined weights.

4.1.1. Economic objective

The economic objective is based on the import costs of the different energy sources from the utility grid in the prediction horizon N_{p}, i.e., electricity ($C^{\text{el}}_{\text{UG}}$), 'green' gas $C^{\text{gas}}_{\text{UG}}$, and hydrogen $C^{\text{hyd}}_{\text{UG}}$. Operational costs due to the increase in maintenance and startup and shut-down costs as in [22] are not considered due to the difficult assumptions that need to be made to approximate these costs in the future microgrid. Therefore, the economic objective is written as

$$J_{\text{eco}} = \sum_{k=1}^{N_{\text{p}}} \left(C^{\text{el}}_{\text{UG}}(k) + C^{\text{gas}}_{\text{UG}}(k) + C^{\text{hyd}}_{\text{UG}}(k) \right).$$

4.1.2. Discomfort objective

The discomfort for the consumers in the microgrid will mainly be influenced by the usage of DR. Furthermore, the range anxiety is included by penalising a lower state of charge of an EV. Another low discomfort is placed on the amount of energy in the battery and hydrogen storage tank. This is penalised in a similar way as for the state of charge of the EVs. The discomfort objective can be written as

$$\begin{aligned} J_{\text{dis}} = \sum_{k=1}^{N_{\text{p}}} \Bigg(& \rho_{\text{c}} \beta_{\text{c}}(k) + \rho^{\text{el}}_{\text{r}} \beta^{\text{el}}_{\text{r}}(k) + \rho^{\text{th}}_{\text{r}} \beta^{\text{th}}_{\text{r}}(k) \\ & + \frac{\rho_{\text{EV}}}{N_{\text{EV}}} \left(\sum_{i=1}^{N_{\text{bev}}} \frac{\overline{x}_{\text{bev},i} - x_{\text{bev},i}(k)}{\overline{x}_{\text{bev},i}} + \sum_{i=1}^{N_{\text{fev}}} \frac{\overline{x}_{\text{fev},i} - x_{\text{fev},i}(k)}{\overline{x}_{\text{fev},i}} \right) \\ & + \rho_{\text{bat}} \frac{\overline{x}_{\text{bat}}(k) - x_{\text{bat}}}{\overline{x}_{\text{bat}}} + \rho_{\text{hst}} \frac{\overline{x}_{\text{hst}} - x_{\text{hst}}(k)}{\overline{x}_{\text{hst}}} \Bigg). \end{aligned}$$

where ρ_{c}, $\rho^{\text{el}}_{\text{r}}$, and $\rho^{\text{th}}_{\text{r}}$ are the penalty weights for curtailment and rescheduling of the electrical and thermal energy, respectively. The parameters ρ_{EV}, ρ_{bat}, and ρ_{hst} are the penalty weights given for the state of charge of the total number of EVs (N_{EV}), the battery, and the hydrogen storage tank, respectively.

4.1.3. Durability objective

Frequent use of the EVs in vehicle-to-grid will result in faster degradation of the batteries and fuel cells in the EVs. Although the degradation is tackled up to a certain degree using the operation constraints, a penalty is still applied to the usage of the EVs in vehicle-to-grid for giving energy to the microgrid to increase its durability as

$$J_{\text{dur}} = \frac{1}{N_{\text{EV}}} \sum_{k=1}^{N_{\text{p}}} \left(\sum_{i=1}^{N_{\text{bev}}} \frac{z^{\text{g}}_{\text{bev},i}(k)}{\overline{z}^{\text{g}}_{\text{bev},i}} + \sum_{i=1}^{N_{\text{fev}}} \frac{u^{\text{el}}_{\text{fev},i}(k)}{\overline{u}^{\text{el}}_{\text{fev},i}} \right),$$

where $z^{\text{g}}_{\text{bev}}(k) = \delta^{\text{g}}_{\text{bev}}(k) u_{\text{bev}}(k)$ is introduced by the mixed logical dynamical modelling [27], where $\delta^{\text{g}}_{\text{bev}}(k)$ indicates whether the battery EV is in generation mode at time step k.

4.1.4. Grid demand objective

The maximum value of the electrical energy exchange per time step is penalised since we want to reduce the increase in energy infrastructure. Therefore, the absolute maximum energy transfer of the electricity needs to be minimised using a weight ρ_{GD}. An auxiliary variable $\zeta^{\text{el}}_{\text{ug}}(k)$ is introduced to obtain a linear objective function using the auxiliary variable $z^{\text{el}}_{\text{UG}}(k) = \delta^{\text{el}}_{\text{UG}}(k) u^{\text{el}}_{\text{UG}}(k)$ as introduced for the mixed logical dynamical modelling. This results in the objective as

$$\begin{aligned} & J_{\text{gd}} = \rho_{\text{GD}} \cdot \max_k |u^{\text{el}}_{\text{UG}}(k)| = \rho_{\text{GD}} \cdot \zeta^{\text{el}}_{\text{ug}}(k), \text{ with} \\ & \quad \zeta^{\text{el}}_{\text{ug}}(k) \geq 2 z^{\text{el}}_{\text{UG}}(k) - u^{\text{el}}_{\text{UG}}(k), \quad k = 1, \ \ldots, \ N_{\text{p}}, \end{aligned}$$

where the lower equation ensures that the value of $\zeta^{\text{el}}_{\text{ug}}(k)$ remains positive for both the import and export of energy.

4.2. Model predictive control

There has been a vast amount of literature on MPC for discrete-time systems where the observable states $\boldsymbol{x}$ and inputs $\boldsymbol{u}$ are constrained, described as

$$\begin{aligned} & \boldsymbol{x}(k+1) = f(\boldsymbol{x}(k), \ \boldsymbol{u}(k)), \quad \boldsymbol{y}(k) = h(\boldsymbol{x}(k)), \boldsymbol{x} \in \mathbb{X}, \ \boldsymbol{u} \in \mathbb{U}, \\ & f \in \mathbb{R}^n \times \mathbb{R}^m \to \mathbb{R}^n, \ \boldsymbol{y} \in \mathbb{R}^b, \text{ and } h \in \mathbb{R}^n, \end{aligned} \tag{2}$$

with $\boldsymbol{x}$ representing the state and $\boldsymbol{y}$ the output of the system. In this paper, the state is assumed to be observable. At each time step, an optimal control problem is solved while simulating the future states in a receding horizon fashion. For the length of this finite-horizon window, i.e., the prediction horizon, an optimal control sequence is computed. This optimal control sequence calculates an optimal control input at each time step in the control horizon window, where the control horizon is always equal or smaller than the prediction horizon. The first control of the computed sequence is implemented in the system and the process is repeated for the next time step.

The main advantage for using MPC, compared to more conventional rule-based control methods, is that this controller is optimisation based. Therefore, a determined cost function can be optimised and better results are obtained. Furthermore, MPC considers the future evolution of the system when determining the optimal control input as well, strengthening the ability to gain an even better performance. Increasing the control horizon can improve the performance of the closed-loop controlled system, but it also increases the computation time.

In this paper, the considered MLD model will result in an mixed-integer linear programming problem. The main drawback of a MLD model using MPC is the computational burden due to the introduction of the binary variables in the optimisation. Such a problem is NP-hard and, loosely speaking, the overall worst-case complexity of mixed-integer problems is exponential in the number of binary optimisation variables [49].

In general, no constraints satisfaction nor recursive feasibility can be guaranteed by using MPC due to the errors in the point forecasts, i.e., violations of the constraints can occur [50]. A low-level controller is therefore implemented in the microgrid to compensate for the discrepancies in the microgrid during the optimisation. The low-level controller imports extra 'green' gas, hydrogen, or electrical energy during a shortage of energy and activates the hybrid heat pumps to generate thermal energy. During an abundance of energy, similar steps are taken, with the difference that the abundance in 'green' gas, hydrogen, or electrical energy is subtracted from the imported quantity. Feasibility is assumed to be ensured since there are no constraints on the imported energy and the hybrid heat pumps can provide more thermal energy than the maximum thermal demand measured in the historic data.

4.3. Control of uncertainty

Extensions on the nominal MPC are possible to deal with the uncertainties of the point forecasts for the stochastic processes better and obtain an improved overall performance of the microgrid. Different robust and stochastic MPC methods that can deal with the nonlinearities of the mixed-integer linear programming problem are briefly elaborated upon for future research.

In robust MPC, the uncertainty is assumed to be bounded and for all required realisations of the disturbances $\boldsymbol{w} = \{w(0),\ w(1), \dots, w(N-1)\} \in \mathbb{W}^N$ the control constraints need to be satisfied [50]. This guarantees feasibility for the bounded disturbances but results in a conservative solution. To decrease the conservatism of the results, stochastic MPC can be used where the constraints are assumed to be stochastic. In this method, the constraints are softened, i.e., the constraints do not need to be satisfied for all possible realisations of the disturbances [50]. In the optimisation of stochastic MPC, a trade-off should be made between the control performance and the probability of state constraint violation [51]. Two stochastic MPC strategies that can be adapted with the nonlinearities of the mixed-integer linear programming problem are [52]: scenario-based and tree-based MPC. These control strategies should be investigated in future work to improve the performance of the microgrid.

5. Case study

In this section, simulations are performed for different case studies. Three scenarios that consider different levels of penetration of hydrogen in the microgrid are defined. From these results, the question of how hydrogen influences the peak of electrical energy transfer of the microgrid and the required grid investments is answered.

5.1. Setup

The number of distributed energy resources and their specifications are based on realistic future investments and calculated ratios as will be presented in following paragraphs.

Buildings. To estimate the energy demand of the microgrid, the number of buildings in the microgrid is chosen. A ratio of 42:1 for residential to small commercial buildings is calculated based on data in Amsterdam, The Netherlands [53]. Therefore, it is chosen to construct a microgrid with 42 residential buildings and one small commercial building. It is chosen not to include more buildings since this will increase the computation time due to an increase of decision variables.

Demand response. In each residential building, a dishwasher, which has an energy consumption of 0.78 kWh and which is used five times a week, is chosen to participate in the DR program as reschedulable load. Furthermore, we assume that 10% of the real consumed thermal energy demand in residential buildings can be rescheduled and another 10% curtailed.

Electric distributed energy resources. PV panels are installed on each building with an average power of 3.34 kW, estimated from the research done in [28]. This yields a 143.62 kW maximum power of solar panels in the microgrid. A district battery with a maximum storage capacity of 500 kWh and a maximum power of 150 kW is considered. It is assumed that the battery does not discharge below 10% of its maximum capacity and has a charging and discharging efficiency of 90%. An electrolyser is used with a maximum power consumption of 25 kW containing an integrated hydrogen storage system with a storage capacity of 500 kg. It is assumed that the storage level does not drop below 5% of the maximum storage. Since an efficiency of the electrolyser of 70% and a heating value of hydrogen of 39.4 kWh/kg [10] are assumed, the model parameter α_{elc} is estimated to be 0.02 kg/kWh.

Thermal distributed energy resources. A hybrid heat pump is installed with a maximum power of 20 kW. The efficiency for the electric part is 400% due to heat obtained from the ground or air. The boiler in the hybrid heat pump that burns gas has an efficiency of 90% for both 'green' gas and hydrogen. Furthermore, a 5 kW μ-CHP plant is installed with a thermal storage capacity of 70 kWh. The efficiency for the electrical energy and thermal energy are 22.5% and 67.5% for the $\mu-$CHP plant with an internal combustion engine, respectively, and both 45% for the $\mu-$CHP plant with a fuel cell.

Electric vehicles. A single EV per household is considered. Battery EVs with a charging and discharging efficiency of 90% and a maximum battery storage capacity of 100 kWh are used. Their charging or discharging power is set to be a maximum of 16 kW. The fuel cell EVs in the microgrid have a fuel storage capacity of 7 kg of hydrogen with a refilling rate of 2 kg/h. Since this EV operates on partial load in the microgrid, the maximum power is set to be at 15 kW. The model parameters α_{FEV} and β_{FEV} for the fuel cell EVs are based on the model of fuel cell stacks in [34] and are determined to be 0.06 kg/kWh and 0.11 kg/h, respectively [10].

5.2. Scenarios

Three scenarios with different levels of penetration of hydrogen in the microgrid are considered. The energy and thermal demand is similar for each scenario. Therefore, a fair comparison can be made about how the introduction of hydrogen in the microgrid will influence the performance. The following three scenarios are considered, schematically visualised in Fig. 1, as:

(1) **Electric**: In this scenario, no hydrogen is present in the microgrid. Therefore, no electrolyser with an integrated hydrogen storage tank and fuel cell EVs are present. The hybrid heat pumps and μ-CHP plant can run on 'green' gas that is imported from the utility grid.
(2) **Mixed**: This scenario is based on the expected microgrid in the Netherlands in 2050 [28]. Both electric and hydrogen-based components are present in the microgrid. However, no 'green' gas is considered since hydrogen will be using the current natural gas infrastructure. Using both gases would lead to an extra gas network which is preferred to be avoided since the extra investments needed will probably overrule the potential profit. Therefore, the hybrid heat pumps and μ-CHP plant will contain fuel cells that run on hydrogen instead of the 'green' gas. Furthermore, the electrolyser with an integrated hydrogen storage tank is included in the microgrid. Both types of EVs are present and a ratio of 1.5:1 for the number of battery EVs to the number of fuel cell EVs is used [28].
(3) **Hydrogen**: In this scenario, a hydrogen-based microgrid is considered. The microgrid consists of almost the same distributed energy resources as in the mixed scenario, with the only difference that the battery is excluded from the microgrid. Furthermore, all the battery EVs are replaced by fuel cell EVs.

5.3. Performance indices

The performance of the energy management of the microgrid is measured by economic and generic performance indices. In the economic performance indices, the performance is measured in terms of economic costs. The generic performance indices are estimated as a value between 0 and 1, yielding a better performance with a higher value. An overview of these different performance indices based on the number of time steps during the simulation T are:

Economic performance indices

- **Electrical grid investment:** The peak of electrical energy transfer is translated to variable economic investments needed to be paid by the energy suppliers following the prices in the Netherlands. Hence, economic costs are based on the peak of electrical energy transfer, i.e., €2.4147 per month per maximum transferred energy in kW [54]. This results in the equation for the electrical grid investment, with T_{m} as the number of time steps in a month, as

$$\mathrm{EGI} = 2.4147 \cdot \frac{T}{T_{\mathrm{m}}} \sum_{k=1}^{T} \left(\zeta_{\mathrm{ug}}^{\mathrm{el}}(k) \right).$$

- **Energy import costs:** The netted economic costs of the microgrid by purchasing and selling energy is calculated as

$$\mathrm{EIC} = \sum_{k=1}^{T} \left(C_{\mathrm{UG}}^{\mathrm{el}}(k) + C_{\mathrm{UG}}^{\mathrm{gas}}(k) + C_{\mathrm{UG}}^{\mathrm{hyd}}(k) \right).$$

Generic performance indices

- **Comfort level:** The discomfort costs in the microgrid are rewritten as a normalised comfort level for the consumers. This comfort level is estimated by considering the comfort decrease due to participation in DR, the influence of range anxiety, and battery state of charge. The comfort level is calculated as the discomfort objective divided by its weights as

$$\mathrm{CL} = 1 - \frac{J_{\mathrm{dis}}}{\rho_{\mathrm{c}} + \rho_{\mathrm{r}}^{\mathrm{el}} + \rho_{\mathrm{r}}^{\mathrm{th}} + \rho_{\mathrm{EV}} + \rho_{\mathrm{bat}} + \rho_{\mathrm{hst}}}.$$

- **Durability of EV:** The durability of the EVs is influenced by the possible intensive usage in vehicle-to-grid and is also penalised in the objective function. A durability ratio for the EVs is calculated that identifies the ratio of vehicle-to-grid used when not on transportation $\left(\delta^{\mathrm{t}}(k) = 0\right)$. The durability ratio for the EVs is calculated as

$$\mathrm{DEV}_{\mathrm{n}} = \sum_{k=1}^{T} \left(\sum_{i=1}^{N_{\mathrm{bev}}} \left(1 - \delta_i^{\mathrm{t}}(k)\right) \frac{z_{\mathrm{bev},i}^{\mathrm{g}}(k)}{\overline{z}_{\mathrm{bev},i}^{\mathrm{g}}} + \sum_{i=1}^{N_{\mathrm{fev}}} \left(1 - \delta_i^{\mathrm{t}}(k)\right) \frac{u_{\mathrm{fev},i}^{\mathrm{el}}(k)}{\overline{u}_{\mathrm{fev},i}^{\mathrm{el}}} \right),$$

$$\mathrm{DEV} = 1 - \frac{\mathrm{DEV}_{\mathrm{n}}}{\sum_{k=1}^{T} \sum_{i=1}^{N_{\mathrm{EV}}} \left(1 - \delta_i^{\mathrm{t}}(k)\right)}.$$

- **Electric self-supply:** A microgrid can be rated by the ability to use the generated energy in the microgrid as proposed in [55–57], i.e., not selling the energy if there is an abundance. The electric self-supply performance index calculates the ratio between the exported and generated electrical energy in the microgrid as

$$\mathrm{ESS} = 1 - \frac{\sum_{k=1}^{T} \left(z_{\mathrm{UG}}^{\mathrm{el}}(k) - u_{\mathrm{UG}}^{\mathrm{el}}(k) \right)}{\sum_{k=1}^{T} \left(P_{\mathrm{PV}}(k) + P_{\mathrm{CHP}}(k) \right)}.$$

- **Energy independence:** The energy independence of a microgrid can be rated by calculating the ratio of imported energy to the consumed energy [55,56,58,59]. The energy independence is a measure for self-reliance of a microgrid. It explains the ability of a microgrid to deal with unexpected excessive demand. The energy independence of the microgrid is calculated as

$$\mathrm{EI}_{\mathrm{d}} = \sum_{k=1}^{T} \Bigg(P_{\mathrm{res}}(k) + P_{\mathrm{com}}(k) + Q_{\mathrm{res}}(k) + Q_{\mathrm{com}}(k) + \sum_{k=1}^{N_{\mathrm{bev}}} \left(h_{\mathrm{bev},i}(k)\right) + \sum_{k=1}^{N_{\mathrm{fev}}} \left(h_{\mathrm{fev},i}(k)\right) \Bigg),$$

$$\mathrm{EI} = 1 - \frac{\sum_{k=1}^{T} \left(z_{\mathrm{UG}}^{\mathrm{el}}(k) + z_{\mathrm{UG}}^{\mathrm{th}}(k) \right)}{\mathrm{EI}_{\mathrm{d}}},$$

where $z_{\mathrm{UG}}^{\mathrm{th}}$ presents the imported gas in kWh and the trip costs h_{bev} and h_{fev} are calculated in kWh as well.

5.4. Simulation weeks

A strong difference for the energy demand and PV power generation throughout the year is observed from the analysis of the stochastic processes. Therefore, it is chosen to simulate a typical winter week and a typical summer week for the Netherlands. These two weeks are analysed, and it is concluded that in an extreme winter week the most energy transfer between the microgrid and utility grid is expected. Hence, a week with extremely cold temperatures is simulated as well to determine the minimum electrical energy grid investments needed to guarantee the reliability of the microgrid. A high thermal energy demand and low PV power, due to the low solar irradiance in the winter, is present this week. From these different weeks, an overview of the average costs during the year can be derived based on the summer and winter case study. Furthermore, the minimum electrical energy grid investments can be determined based on the week with extreme conditions.

Each simulation in the different microgrids consists of eight consecutive days where the first day is only used for initialisation to create a more realistic initial values for the energy stored in the distributed energy resources. Thus, the results are based on the last seven days of the simulation. The simulation starts on a Monday and ends on the next Monday. It is chosen to use this order to include the influence of the weekend on the first weekday. In Fig. 2, the energy transfer between the microgrid and utility grid is shown as example.

The mixed-integer linear programming problem for the MLD-MPC optimisation is solved in the Matlab R2020a environment using Gurobi [60]. An HP EliteBook 8570w with a 2.3 GHz Intel Core i7 processor and 4 GB of RAM is used for the simulations. Different computation times are obtained for the controllers in each case study and scenario. In general, the computation time increases with a higher energy demand in the case study. The computation time for the week with extreme conditions is approximately 3 h.

5.5. Results

Fig. 2 shows the energy transfer between the microgrid and utility grid during the simulations. In Table 1, the system performance for the different scenarios in these simulations is presented. It is shown that a general trend is present for each week between the scenarios. A higher level of hydrogen penetration in the microgrid reduces the peak of electrical energy transfer of the microgrid, as shown in the costs of EGI and Fig. 2. However, the total economic costs increase due to the higher energy import costs, as seen in the Total costs column. These higher energy import costs are mainly due to the more expensive fuel costs for fuel cell EVs compared to battery EVs. The fuel costs are more expensive due to the higher import price of hydrogen compared to electrical energy and the low efficiency in the fuel cells. It must be noted that the expected hydrogen price and low efficiency of the fuel cells influence the results of the optimisation substantially and future research should focus on improving hydrogen technology such that the efficiency grows and the price drops.

The electrical energy grid investments are based on the week with extreme conditions. The energy import costs are calculated by averaging the costs in the typical winter and summer weeks, representing an approximation of the mean costs throughout the year. It is concluded that a reduction in the electrical grid investments of 16.90% and 81.29% is achieved for the mixed and hydrogen scenario as seen in Table 1 in the column presenting the costs of EGI, respectively. However, the total economic costs are increased for the mixed and hydrogen scenario, respectively by 29.92% and 52.38% as seen in the column 'Total costs'. Therefore, despite reducing the grid investment costs, introducing hydrogen to the microgrid will still lead to more economic costs.

The introduction of hydrogen results in a lower energy independence of the microgrid, decreasing the self-reliance of the microgrid.

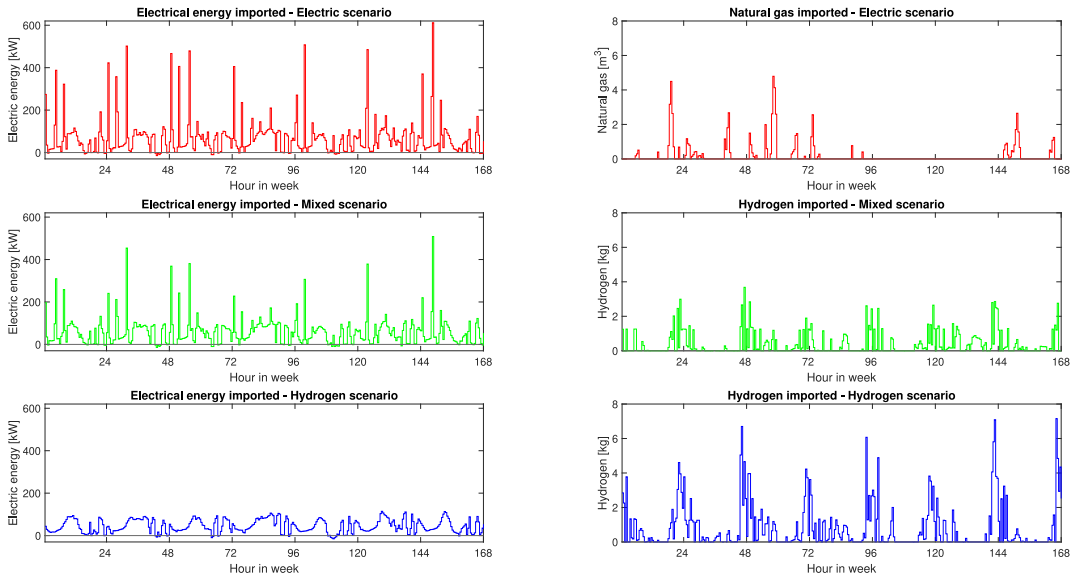

Fig. 2. Energy transfer between the microgrid and utility grid in the different scenarios for the extreme conditions case study.

Table 1
The results on the performance indices for the scenarios in the different weeks.

Week	Scenario	EGI [€]	EIC [€]	Total costs [€]	CL	DEV [10^3]	ESS	EI	Total objective costs
Summer	Electric	271	53	324	0.8826	0.6795	0.7973	0.7073	14
	Mixed	173	211	384	0.7432	0.6349	0.8007	0.3831	22
	Hydrogen	34	511	545	0.8258	0.8031	0.8034	0.1347	39
Winter	Electric	338	409	747	0.6379	0.7554	0.8448	0.5956	47
	Mixed	239	711	950	0.5873	0.6230	0.8414	0.5171	67
	Hydrogen	48	1115	1163	0.6320	0.7424	0.8660	0.4075	92
Extreme conditions	Electric	345	548	893	0.4537	0.7648	0.9478	0.6760	60
	Mixed	286	850	1136	0.4306	0.6450	0.9402	0.6081	82
	Hydrogen	64	1257	1321	0.4624	0.7497	0.9618	0.5406	106

This is due to the lower efficiency of the fuel cell compared to the battery and more devices running on hydrogen, which is mainly imported. Another trend is that for the mixed scenario including both battery and fuel cell EVs, more degradation will occur on the battery and fuel cells of the EVs due to the higher use of the EVs in vehicle-to-grid operations. Furthermore, in the mixed scenario, a lower comfort level is obtained due to the lower state of charge of the EVs. No clear differences are concluded for the self-supply of the microgrids since different trends are seen for the ESS in Table 1 between the levels of hydrogen penetration in the different weeks.

6. Conclusions

In this paper, the influence of hydrogen on the electrical grid investments costs has been analysed. A simulation-based case study has been performed where scenarios with different levels of hydrogen have been compared. It is shown that the introduction of hydrogen in the microgrid reduces the electrical grid investments costs for the mixed and hydrogen scenario with 16.90% and 81.29% while yielding higher energy import costs, increasing the total economic costs by 29.92% and 52.38%, respectively. Furthermore, the introduction of hydrogen in the microgrid shows a clear decrease in the energy independency of the microgrid. In a microgrid containing both battery and fuel cell EVs, it is concluded that more vehicle-to-grid operations are used compared to the microgrids including only one type of EV. In conclusion, an increase in the level of hydrogen in the microgrid will reduce the electric grid investments costs but is not economically more beneficial than using 'green' gas.

As future work, unknown departure times need to be considered, i.e., forecasting models need to be developed to predict the behaviour of the arrival and departure times of the EVs instead of assuming them to be known beforehand.

Furthermore, stochastic MPC methods that can deal with the non-linearities of the mixed-integer linear programming problem (e.g., scenario- and tree-based MPC) can be evaluated to see if better performance of the microgrid can be reached. With these methods, it is possible to include the uncertainties in the point forecasting in the control of the microgrid.

Another aspect is that scaling the size of the microgrid could influence the performance of the microgrid. Therefore, the influence of hydrogen on smaller and larger microgrids should be evaluated. Since the computational complexity rises when increasing the size of the microgrid, alternative techniques as distributed MPC [61] or parameterised MPC [62] could be considered to decrease the number of decision variables and, therefore, the computational complexity and computation time needed.

Lastly, the results of the experiments can be strengthened by using statistical tests to evaluate the results and including reliability parameters in the optimisation of the microgrid. These aspects contribute to be able to construct a complete picture of the influences of hydrogen in the microgrid.

Declaration of competing interest

The authors declare that they have no known competing financial interests or personal relationships that could have appeared to influence the work reported in this paper.

References

[1] United Nations. Adoption of the Paris agreement. 2019, http://unfccc.int/files/essential_background/convention/application/pdf/english_paris_agreement.pdf. Accessed: 14-December-2019.

[2] Hirsch A, Parag Y, Guerrero J. Microgrids: A review of technologies, key drivers, and outstanding issues. Renew Sustain Energy Rev 2018;90:402–11.

[3] Lago J, De Brabandere K, De Ridder F, De Schutter B. Short-term forecasting of solar irradiance without local telemetry: A generalized model using satellite data. Sol Energy 2018;173:566–77.

[4] Farahani SS, van der Veen R, Oldenbroek V, Alavi F, Lee EHP, van de Wouw N, et al. A hydrogen-based integrated energy and transport system: The design and analysis of the car as power plant concept. IEEE Syst Man Cybern Mag 2019;5(1):37–50.

[5] Zakariazadeh A, Jadid S, Siano P. Smart microgrid energy and reserve scheduling with demand response using stochastic optimization. Int J Electr Power Energy Syst 2014;63:523–33.

[6] Korkas CD, Baldi S, Michailidis I, Kosmatopoulos EB. Occupancy-based demand response and thermal comfort optimization in microgrids with renewable energy sources and energy storage. Appl Energy 2016;163:93–104.

[7] Kumar Nunna HSVS, Doolla S. Demand response in smart distribution system with multiple microgrids. IEEE Trans Smart Grid 2012;3(4):1641–9.

[8] Mukherjee JC, Gupta A. A review of charge scheduling of electric vehicles in smart grid. IEEE Syst J 2014;9(4):1541–53.

[9] Yildiz B, Bilbao JI, Sproul AB. A review and analysis of regression and machine learning models on commercial building electricity load forecasting. Renew Sustain Energy Rev 2017;73:1104–22.

[10] Alavi F, Lee EP, van de Wouw N, De Schutter B, Lukszo Z. Fuel cell cars in a microgrid for synergies between hydrogen and electricity networks. Appl Energy 2017;192:296–304.

[11] Geske J, Schumann D. Willing to participate in vehicle-to-grid (V2G)? Why not!. Energy Policy 2018;120:392–401.

[12] Tahmasebi M, Ghadiri A, Haghifam MR, Miri-Larimi SM. Mpc-based approach for online coordination of EVs considering EV usage uncertainty. Int J Electr Power Energy Syst 2021;130:106931.

[13] Moradmand A, Dorostian M, Shafai B. Energy scheduling for residential distributed energy resources with uncertainties using model-based predictive control. Int J Electr Power Energy Syst 2021;132:107074.

[14] Velasquez MA, Barreiro-Gomez J, Quijano N, Cadena AI, Shahidehpour M. Distributed model predictive control for economic dispatch of power systems with high penetration of renewable energy resources. Int J Electr Power Energy Syst 2019;113:607–17.

[15] Siano P. Demand response and smart grids - a survey. Renew Sustain Energy Rev 2014;30:461–78.

[16] Manoharan Y, Hosseini SE, Butler B, Alzhahrani H, Senior BTF, Ashuri T, Krohn J. Hydrogen fuel cell vehicles; current status and future prospect. Appl Sci 2019;9(11):2296.

[17] Wei F, Sui Q, Li X, Lin X, Li Z. Optimal dispatching of power grid integrating wind-hydrogen systems. Int J Electr Power Energy Syst 2021;125:106489.

[18] Lai JS, Ellis MW. Fuel cell power systems and applications. Proc IEEE 2017;105(11):2166–90.

[19] Thomas CE. Fuel cell and battery electric vehicles compared. Int J Hydrog Energy 2009;34(15):6005–20.

[20] Li Q, Chen W, Li Y, Liu S, Huang J. Energy management strategy for fuel cell/battery/ultracapacitor hybrid vehicle based on fuzzy logic. Int J Electr Power Energy Syst 2012;43(1):514–25.

[21] Velarde P, Valverde L, Maestre JM, Ocampo-Martínez C, Bordons C. On the comparison of stochastic model predictive control strategies applied to a hydrogen-based microgrid. J Power Sources 2017;343:161–73.

[22] Parisio A, Rikos E, Glielmo L. A model predictive control approach to microgrid operation optimization. IEEE Trans Control Syst Technol 2014;22(5):1813–27.

[23] Bartolucci L, Cordiner S, Mulone V, Santarelli M. Hybrid renewable energy systems: Influence of short term forecasting on model predictive control performance. Energy 2019;172:997–1004.

[24] Bolzoni A, Parisio A, Todd R, Forsyth A. Model predictive control for optimizing the flexibility of sustainable energy assets: An experimental case study. Int J Electr Power Energy Syst 2021;129:106822.

[25] del Real AJ, Arce A, Bordons C. Combined environmental and economic dispatch of smart grids using distributed model predictive control. Int J Electr Power Energy Syst 2014;54:65–76.

[26] Blaud PC, Haurant P, Claveau F, Lacarrière B, Chevrel P, Mouraud A. Modelling and control of multi-energy systems through multi-prosumer node and economic model predictive control. Int J Electr Power Energy Syst 2020;118:105778.

[27] Bemporad A, Morari M. Control of systems integrating logic, dynamics, and constraints. Automatica 1999;35(3):407–27.

[28] Berenschot, Kalavasta. Klimaatneutrale energiescenario's 2050, [ENG]: Climate neutral energy scenarios 2050. 2020.

[29] Fathima AH, Palanisamy K. Optimization in microgrids with hybrid energy systems – a review. Renew Sustain Energy Rev 2015;45:431–46.

[30] Riordan C, Hulstron R. What is an air mass 1.5 spectrum? (solar cell performance calculations). In: IEEE Conference On Photovoltaic Specialists. IEEE; 1990, p. 1085–8.

[31] Liu C, Chau KT, Wu D, Gao S. Opportunities and challenges of vehicle-to-home, vehicle-to-vehicle, and vehicle-to-grid technologies. Proc IEEE 2013;101(11):2409–27.

[32] Van Der Kam M, van Sark W. Smart charging of electric vehicles with photovoltaic power and vehicle-to-grid technology in a microgrid; a case study. Appl Energy 2015;152:20–30.

[33] Corchero C, Cruz-Zambrano M, Heredia FJ, et al. Optimal energy management for a residential microgrid including a vehicle-to-grid system. IEEE Trans Smart Grid 2014;5(4):2163–72.

[34] Rodatz P, Paganelli G, Sciarretta A, Guzzella L. Optimal power management of an experimental fuel cell/supercapacitor-powered hybrid vehicle. Control Eng Pract 2005;13(1):41–53.

[35] ElaadNL. Open datasets. 2020, Available: https://platform.elaad.io/download-data/. Accessed: 20-November-2020.

[36] Refa N, Hubbers N. Impact of smart charging on EVs charging behaviour assessed from real charging Event, in: 32nd Electric Vehicle Symposium, 2019.

[37] Das UK, Tey KS, Seyedmahmoudian M, Mekhilef S, Idris MYI, Van Deventer W, Horan B, Stojcevski A. Forecasting of photovoltaic power generation and model optimization: A review. Renew Sustain Energy Rev 2018;81:912–28.

[38] Jung J, Broadwater RP. Current status and future advances for wind speed and power forecasting. Renew Sustain Energy Rev 2014;31:762–77.

[39] Vagropoulos SI, Chouliaras GI, Kardakos EG, Simoglou CK, Bakirtzis AG. Comparison of SARIMAX, SARIMA, modified SARIMA and ANN-based models for short-term PV generation forecasting, in: IEEE International Energy Conference, 2016, 1–6.

[40] Box GEP, Jenkins GM, Reinsel GC. Time Series Analysis, Forecasting And Control. Holden Day; 1976.

[41] Wan C, Zhao J, Song Y, Xu Z, Lin J, Hu Z. Photovoltaic and solar power forecasting for smart grid energy management. CSEE J Power Energy Syst 2015;1(4):38–46.

[42] Gou P, Yu J. A nonlinear ANN equalizer with mini-batch gradient descent in 40gbaud PAM-8 IM/DD system. Opt Fiber Technol, Mater Devices Syst 2018;46:113–7.

[43] Hochreiter S, Schmidhuber J. Long short-term memory. Neural Comput 1997;9(8):1735–80.

[44] Kong W, Dong ZY, Jia Y, Hill DJ, Xu Y, Zhang Y. Short-term residential load forecasting based on LSTM recurrent neural network. IEEE Trans Smart Grid 2017;10(1):841–51.

[45] Bacher P, Madsen H, Nielsen HA. Online short-term solar power forecasting. Sol Energy 2009;83(10):1772–83.

[46] Elsinga B, van Sark WGJHM. Short-term peer-to-peer solar forecasting in a network of photovoltaic systems. Appl Energy 2017;206:1464–83.

[47] Antoñanzas J, Osorio N, Escobar R, Urraca R, Martinez-de Pison FJ, Antonanzas-Torres F. Review of photovoltaic power forecasting. Sol Energy 2016;136:78–111.

[48] Agüera-Pérez A, Palomares-Salas JC, de la Rosa JJG, Florencias-Oliveros O. Weather forecasts for microgrid energy management: Review, discussion and recommendations. Appl Energy 2018;228:265–78.

[49] Camacho EF, Ramírez DR, Limón D, De La Peña DM, Alamo T. Model predictive control techniques for hybrid systems. Ann Rev Control 2010;34(1):21–31.

[50] Mayne DQ. Model predictive control: Recent developments and future promise. Automatica 2014;50(12):2967–86.

[51] Heirung TAN, Paulson JA, O'Leary J, Mesbah A. Stochastic model predictive control – how does it work? Comput Chem Eng 2018;114:158–70.

[52] Farina M, Giulioni L, Scattolini R. Stochastic linear model predictive control with chance constraints – a review. J Process Control 2016;44:53–67.

[53] AlleCijfers.nl, Informatie gemeente Amsterdam, [ENG]: Information municipality Amsterdam. 2020, Available: https://allecijfers.nl/gemeente/amsterdam/. [In Dutch], Accessed: 04-August-2020.

[54] Stedin. Tarieven 2020 elektriciteit grootverbruik, [ENG]: Rates 2020 electricity large consumption. 2020, Available: https://www.stedin.net/zakelijk/betalingen-en-facturen/tarieven. [In Dutch], Accessed: 6-October-2020.

[55] Carli R, Cavone G, Pippia T, De Schutter B, Dotoli M. A robust MPC energy scheduling strategy for multi-carrier microgrids. In: International Conference On Automation Science And Engineering. IEEE; 2020, p. 152–8.

[56] Carli R, Dotoli M, Jantzen J, Kristensen M, Othman SB. Energy scheduling of a smart microgrid with shared photovoltaic panels and storage: The case of the ballen marina in samsø. Energy 2020;198:117188.

[57] Hanna R, Ghonima M, Kleissl J, Tynan G, Victor DG. Evaluating business models for microgrids: Interactions of technology and policy. Energy Policy 2017;103:47–61.

[58] Kim M, Parkt S, Choi JK, Lee J. Energy independence of energy trading system in microgrid. In: Innovative Smart Grid Technologies. IEEE; 2017, p. 1–4.

[59] Karimi H, Jadid S. Optimal energy management for multi-microgrid considering demand response programs: A stochastic multi-objective framework. Energy 2020;195:116992.

[60] Gurobi Optimization Inc. Gurobi optimizer reference manual. 2016, https://www.gurobi.com.

[61] Zheng Y, Li S, Tan R. Distributed model predictive control for on-connected microgrid power management. IEEE Trans Control Syst Technol 2017;26(3):1028–39.

[62] Pippia T, Sijs J, De Schutter B. A parametrized model predictive control approach for microgrids, in: IEEE Conference on Decision and Control, 2018, 3171–3176.